Materials Chemistry Horizons RESEARCH

Silica-Supported Magnetic Nanoparticles Functionalized with Phosphorus Species (Fe_3O_4@SiO_2–O–PCl_2): An Efficient and Recyclable Catalyst for the One-Pot Synthesis of Isatin-Based Imidazoles under Mild and Green Conditions

Somayeh Zare, Arezu Jamalian*, Masoomeh Emadi

Department of Chemistry, Marv.C., Islamic Azad University, Marvdasht, Iran
***Corresponding author**: jamalian@iau.ac.ir (A. Jamalian)

Mater. Chem. Horizons, 2026, 5(1), 1-13 10.22128/mch.2026.3386.1073 OPEN ACCESS

ABSTRACT

The synthesis, characterization, and catalytic activity of a novel magnetic nanocatalyst based on phosphorus-functionalized silica-coated iron oxide nanoparticles (Fe_3O_4@SiO_2–O–PCl_2) are described. The prepared nanocatalyst was characterized using FTIR, XRD, VSM, TGA/DTG, FESEM, SEM–EDX, and mapping techniques. Its catalytic performance was evaluated in a one-pot three-component reaction of aromatic aldehydes, isatin, and ammonium acetate to afford a series of substituted 2-phenyl-3,4-dihydroimidazo[4,5-b]indoles with yields of up to 90%. The method offers several advantages, including mild reaction conditions, short reaction times (1 h), high product yields, and excellent catalyst reusability (up to 5 cycles with only a slight loss of activity). The magnetic nature of the catalyst enables facile recovery using an external magnet, making this protocol economically and environmentally benign.

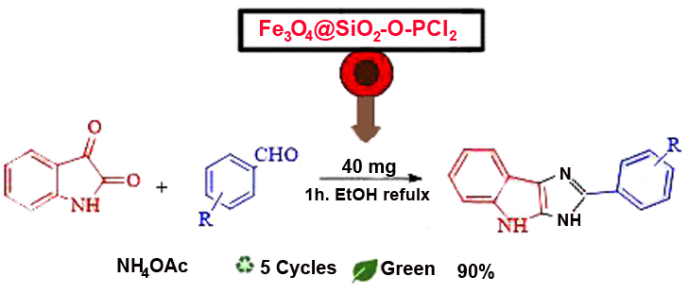

Keywords: 2-Phenyl-3,4-dihydroimidazo[4,5-b]indoles, Heterocyclic compounds, Multicomponent reactions

1. Introduction

In recent years, the demand for knowledge-based design and synthesis of task-specific, biologically-relevant catalysts has grown significantly, as catalytic systems play a key role in pollution prevention [1]. A wide range of solid catalysts, including supported forms, have been documented for various chemical processes [2]. Among these, heterogeneous catalysts offer easy separation from products, eliminating the need for extensive washing [3], and provide advantages such as recyclability and reusability over homogeneous systems. One approach involves attaching a homogeneous catalytic moiety to a nanomagnetic hybrid solid, thereby creating a heterogeneous catalyst capable of performing homogeneous-type tasks [4]. Among the four classes of magnetic nanoparticles—metals, alloys, metal oxides, and ferrites—iron oxides are most studied due to their straightforward preparation and strong magnetic properties. However, ensuring long-term stability remains challenging due to aggregation or surface oxidation [5–8].Multicomponent reactions (MCRs) are highly valuable in synthetic organic chemistry, offering atom efficiency, convergence, and high bond-forming index (BFI). Reactions such as Ugi [9], Passerini [10], Strecker [11], Hantzsch [12], and Biginelli [13] are among the most effective methods for synthesizing heterocycles. Multi-heterocyclic compounds, formed by combining two or more biologically active frameworks [14], are promising candidates for drug discovery [15].The imidazole pharmacophore is a vital class of heterocycles found in many natural products, with derivatives displaying antibacterial [16], proton pump inhibitory (clonidine) [17], antitumor (moxonidine) [17], benzodiazepine antagonist (flumazenil) [18], antifungal [3], antihistaminic (cimetidine) [19], anticancer [20], analgesic [21], antitubercular [22], and antihypertensive [23] activities (**Figure 1**). For a comprehensive overview of imidazole pharmacology, see reference [23].

Received: July 07, 2026
Received in revised: July 22, 2026
Accepted: July 23, 2026

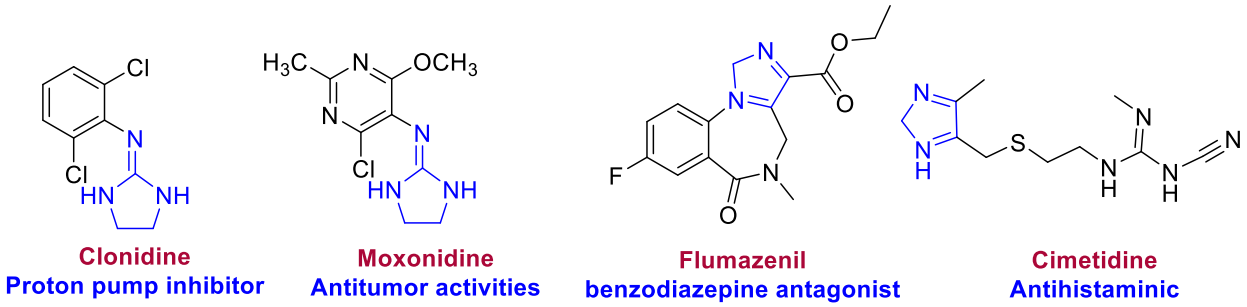

Figure 1. Drug molecules scaffolds bearing imidazole moiety.

Various acidic and basic catalysts have been reported for imidazole synthesis, including $ZrCl_4$ [24], $Yb(OTf)_3$ [25], nanozirconia [26], boric acid with ultrasound [27], L-proline [28], potassium dihydrogen phosphate [29], β-cyclodextrin [30], silica sulfuric acid [25], sodium bisulfite [28], and cerium-immobilized silicotungstic acid on zirconia (Ce@STANPs/ZrO_2) [31]. However, many of these protocols suffer from non-recyclability, toxic solvents, low yields, high temperatures, or long reaction times.To overcome these limitations and in continuation of our interest in silica-based phosphine (silphos) catalysts [32a–c], we now report a silica-supported magnetic nanoparticles-based phosphorus catalyst (Fe_3O_4@SiO_2–O–PCl_2). This new magnetic version offers several distinct advantages over the parent silphos system: (i) facile recovery by an external magnet without the need for filtration or centrifugation, (ii) improved catalytic efficiency due to better dispersion of active sites on the magnetic core, and (iii) excellent reusability for up to five cycles with minimal loss of activity. These features make it a greener and more practical alternative for the synthesis of isatin-based imidazoles (**Scheme 1**). Although PCl_3 is a toxic reagent, it is used in a catalytic amount (1 g per batch) and is covalently anchored to the silica surface, significantly reducing its environmental impact. Moreover, the catalyst is fully recoverable and reusable, minimizing waste generation.

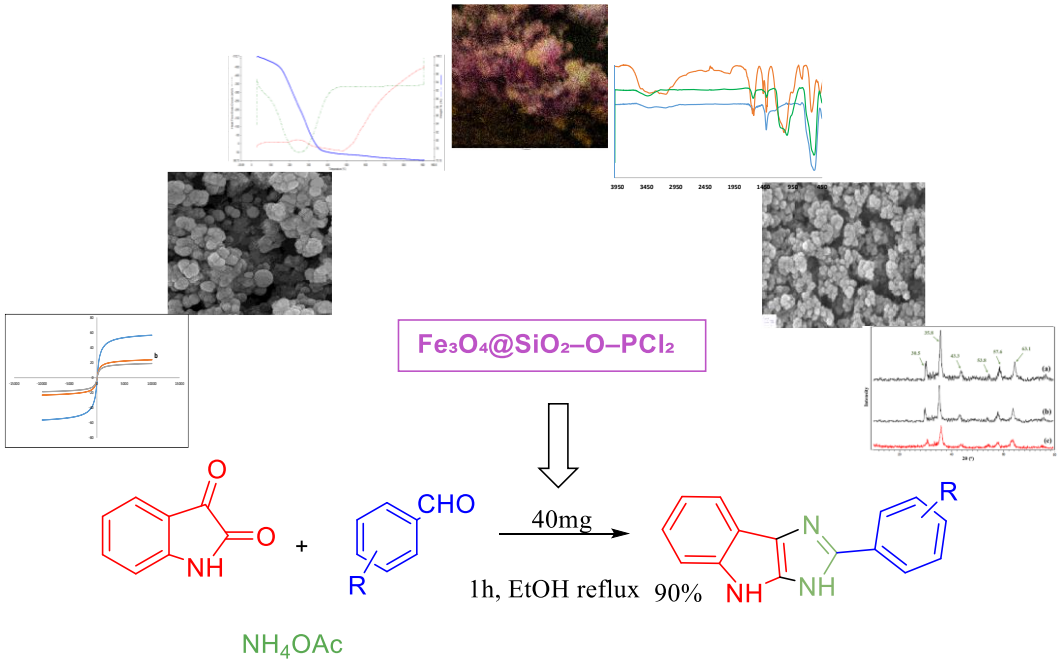

Scheme 1. One-pot multicomponent preparation derivates of 2-phenyl-3,4-dihydroimidazo[4,5-b]indoles catalyzed by Fe_3O_4@SiO_2–O–PCl_2 nanoparticles.

2. Experimental section

2.1. General

Iron(III) chloride ($FeCl_3·6H_2O$), iron(II) chloride ($FeCl_2·4H_2O$), ammonium hydroxide (NH_4OH), aromatic aldehydes, isatin, ammonium acetate, and all other solvents were purchased from Sigma-Aldrich and used without further purification. FT-IR spectra were recorded on a Perkin-Elmer Spectrum Two using KBr pellets (4000–500 cm^{-1}). XRD patterns were collected on a Rigaku D/Max 2500 V with Co Kα radiation (λ = 1.789 Å). VSM measurements were performed on a Zeiss EM900 at room temperature. SEM–EDX analyses were carried out using a Zeiss Sigma/up instrument. TGA/DTG was performed on a Perkin-Elmer TGA-7 under a nitrogen atmosphere (heating rate 10 °C min^{-1}). ^1H NMR (400 MHz) and ^{13}C NMR (100 MHz) spectra were recorded on a Bruker spectrometer using DMSO-d_6 as solvent and TMS as internal standard. Melting points were determined on a Buchi B-545 apparatus and are uncorrected. The syntheses of Fe_3O_4 [7], Fe_3O_4@SiO_2 [7], and the general multicomponent reaction [30] were adapted from literature procedures with minor modifications, as described below.

2.2. Preparation of the magnetic nanocatalyst (Fe_3O_4@SiO_2–O–PCl_2)

2.2.1. Synthesis of Fe_3O_4 nanoparticles

Fe_3O_4 was synthesized following a published coprecipitation method [7]. Briefly, 11.0 g of $FeCl_3·6H_2O$ and 4.0 g of $FeCl_2·4H_2O$ were dissolved in 250 mL of deionized water under vigorous stirring at 25 °C under nitrogen. The pH was adjusted to 9 by dropwise addition of concentrated NH_4OH. The mixture was stirred for an additional 4 h. The black precipitate was magnetically collected, washed repeatedly with deionized water and ethanol until neutral pH, and dried under vacuum at 60 °C.

2.2.2. Synthesis of Fe_3O_4@SiO_2 core–shell nanoparticles

Silica coating was performed via a sol–gel process [7]. In a typical run, 3.0 g of Fe_3O_4 nanoparticles were dispersed in 200 mL of ethanol by ultrasonication for 20 min. Then, 9 mL of concentrated NH_4OH and 8.0 mL of tetraethoxysilane (TEOS) (corrected from an earlier typographical error of 80 mL) were added dropwise. The mixture was stirred at 40 °C for 24 h. The resulting Fe_3O_4@SiO_2 was magnetically separated, washed with water until neutral, then with ethanol and diethyl ether, and dried under vacuum.

2.2.3. Functionalization with phosphorus species (Fe_3O_4@SiO_2–O–PCl_2)

In a dry round-bottom flask under argon atmosphere, 1.0 g of Fe_3O_4@SiO_2 was placed. Then, 20 mL of phosphorus trichloride (PCl_3) was slowly added. The mixture was stirred at room temperature for 1 h under argon. After completion, the solid was filtered, washed several times with dry dichloromethane (50 mL) to remove excess PCl_3, and dried under argon flow, yielding a white/cream solid (2.3 g). The product was stored under inert atmosphere. The PCl_3 reacts with surface silanol (Si–OH) groups to form Si–O–PCl_2 linkages, as confirmed by FT-IR (see Section 3.1.1).

2.3. General procedure for the synthesis of 2-phenyl-3,4-dihydroimidazo[4,5-b]indoles (4a–j)

A mixture of aromatic aldehyde (1 mmol), isatin (1 mmol), ammonium acetate (2 mmol), and Fe_3O_4@SiO_2–O–PCl_2 (40 mg) in ethanol (8 mL) was heated under reflux for 1 hour (optimized time; see **Table 1**). The progress was monitored by TLC (n-hexane/ethyl acetate, 4:1). After completion, the mixture was cooled to room temperature, ethanol (10 mL) was added, and the catalyst was magnetically separated. The filtrate was concentrated and the crude product was crystallized from ethanol to afford pure products. The catalyst was washed with chloroform, dried, and reused for subsequent runs.

Representative spectroscopic data for selected compounds:

2-(p-tolyl)-3,4-dihydroimidazo[4,5-b]indole **(4a)**

Yield: 90%; M.p.: 275–277 °C; FT-IR (KBr, cm^{-1}): 3420 (NH), 3050 (Ar-H), 2920 (CH_3), 1615 (C=N), 1480, 1350, 820; ^1H NMR (DMSO-d_6, 400 MHz): δ 9.16 (s, 1H, NH), 8.24 (s, 1H, NH), 8.04–8.00 (m, 4H, Ar-H), 7.53–7.51 (m,

2H, Ar-H), 7.45–7.41 (m, 2H, Ar-H), 2.42 (s, 3H, CH_3); ^{13}C NMR (DMSO-d_6, 100 MHz): δ 167.95, 150.18, 135.14, 131.79, 130.34, 129.85, 129.04, 126.56, 123.62, 120.40, 115.51, 21.41.

2-(4-chlorophenyl)-3,4-dihydroimidazo[4,5-b]indole **(4b)**

Yield: 87%; M.p.: 282–284 °C; ^1H NMR (DMSO-d_6, 400 MHz): δ 9.20 (s, 1H, NH), 8.30 (s, 1H, NH), 8.10 (d, J = 8.4 Hz, 2H), 7.65 (d, J = 8.4 Hz, 2H), 7.55–7.45 (m, 4H); ^{13}C NMR (DMSO-d_6, 100 MHz): δ 166.8, 150.2, 134.5, 133.2, 131.0, 130.5, 129.0, 128.8, 126.2, 123.5, 120.1, 115.3.

2-(4-nitrophenyl)-3,4-dihydroimidazo[4,5-b]indole **(4c)**

Yield: 85%; M.p.: 295–297 °C; ^1H NMR (DMSO-d_6, 400 MHz): δ 9.30 (s, 1H, NH), 8.45 (s, 1H, NH), 8.35 (d, J = 8.8 Hz, 2H), 8.20 (d, J = 8.8 Hz, 2H), 7.60–7.50 (m, 4H); ^{13}C NMR (DMSO-d_6, 100 MHz): δ 167.2, 150.5, 147.5, 140.0, 135.0, 131.5, 130.0, 127.5, 124.2, 121.0, 116.0.

(Full NMR, IR, and melting point data for all compounds 4a–j are provided in the **Supporting Information**)

3. Results and discussion

3.1. Characterization of the nanocatalyst

3.1.1. FT-IR spectroscopy

Figure 2 presents the FT-IR spectra of Fe_3O_4 (a), Fe_3O_4@SiO_2 (b), and Fe_3O_4@SiO_2–O–PCl_2 (c). The strong bands at 572 and 810 cm^{-1} are characteristic Fe–O vibrations, confirming the Fe_3O_4 core [33]. A broad band near 3400 cm^{-1} and a weak band at 1616 cm^{-1} are attributed to Fe–OH groups (Figure 2a). In the silica-coated sample (Figure 2b), a broad band around 1054 cm^{-1} corresponds to Si–O stretching, while the band at 3424 cm^{-1} is assigned to Si–OH vibrations [34]. In the final catalyst (Figure 2c), the band at ~1411 cm^{-1} is assigned to P–O–Si stretching [35], confirming successful covalent attachment of PCl_3 to the silica surface via condensation with surface silanol groups. Importantly, the P–Cl stretching vibration typically appears at 450–580 cm^{-1} [36]; its absence in the spectrum indicates complete hydrolysis/condensation to P–O–Si linkages, meaning the active species is a surface-bound phosphorus oxychloride derivative rather than free PCl_3.

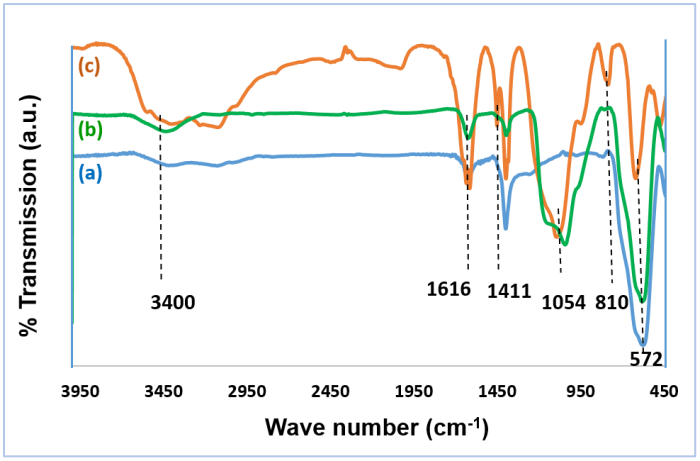

Figure 2. FT-IR spectra of: (**a**) Fe_3O_4, (**b**) Fe_3O_4@SiO_2, (**c**) Fe_3O_4@SiO_2–O–PCl_2

3.1.2. TGA/DTG analysis

Thermogravimetric analysis (**Figure 3**) shows that the catalyst is thermally stable up to 300–350 °C; above this temperature, decomposition occurs rapidly, with a total weight loss of 25.47% [37]. This high thermal stability ensures that the catalyst retains its activity under the reaction conditions without significant degradation of the active species.

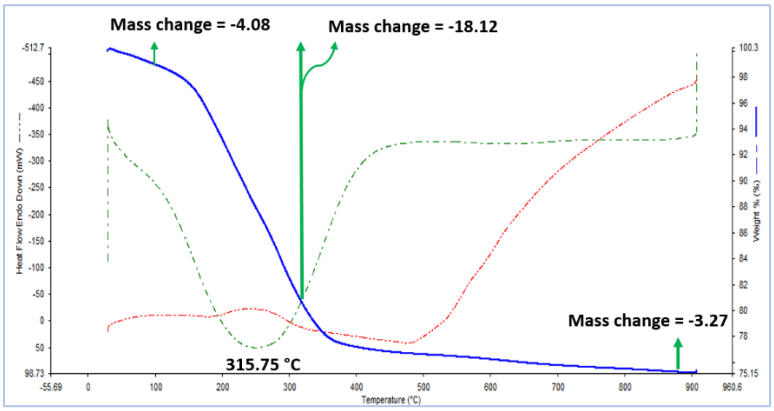

Figure 3. TGA/DTG analysis of Fe_3O_4@SiO_2–O–PCl_2 catalyst.

3.1.3 XRD analysis

XRD patterns (**Figure 4**) display characteristic peaks of spinel ferrites (JCPDS card no. 85-1436) [38], confirming that the crystalline Fe_3O_4 core remains intact after silica coating and phosphorus functionalization. The major peaks at 2θ = 30.50°, 35.80°, 43.30°, 53.80°, 57.60°, and 63.10° correspond to the (220), (311), (400), (422), (440), and (511) planes, respectively. No additional peaks from crystalline silica or phosphorus species are observed, indicating that the silica coating is amorphous and the phosphorus is covalently bound to the surface rather than forming a separate crystalline phase.

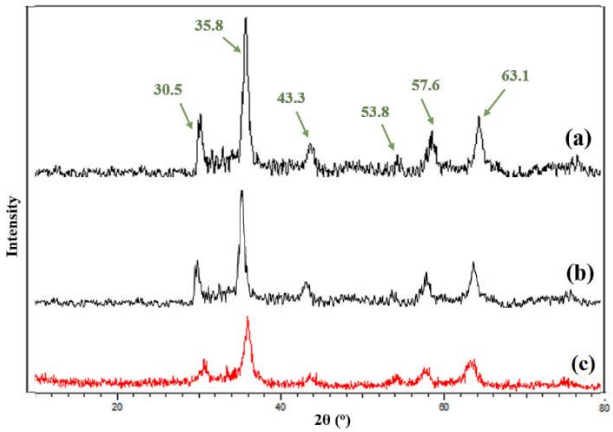

Figure 4. X-ray diffraction patterns of: (**a**) Fe_3O_4, (**b**) Fe_3O_4@SiO_2, (**c**) Fe_3O_4@SiO_2–O–PCl_2

3.1.4. SEM-EDX and mapping

SEM images (**Figure 5**) show relatively uniform nanoparticle morphology with slight agglomeration, typical for nanomaterials. EDX analysis (**Figure 6** and **Table 1**) confirms the presence of Fe, O, Si, P, and Cl. The Si content (15.30 wt%) is consistent with a thin, uniform silica coating obtained using 8.0 mL TEOS (corrected amount). This Si content is reasonable for a monolayer or sub-monolayer coating, as opposed to the formation of bulk silica gel that would occur with 80 mL TEOS. The P content (3.35 wt%) and Cl content (1.45 wt%) indicate successful surface functionalization with phosphorus species. Mapping analysis (**Figure 7**) demonstrates homogeneous distribution of all elements across the nanoparticle surface.

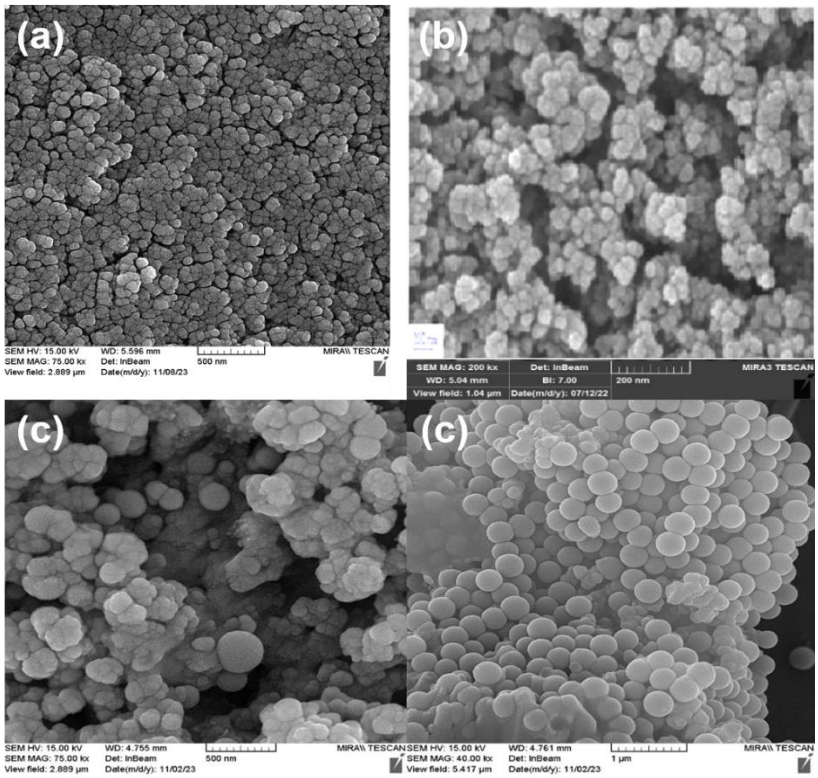

Figure 5. FE-SEM images: (**a**) Fe_3O_4; (**b**) Fe_3O_4@SiO_2; (**c**) Fe_3O_4@SiO_2–O–PCl_2

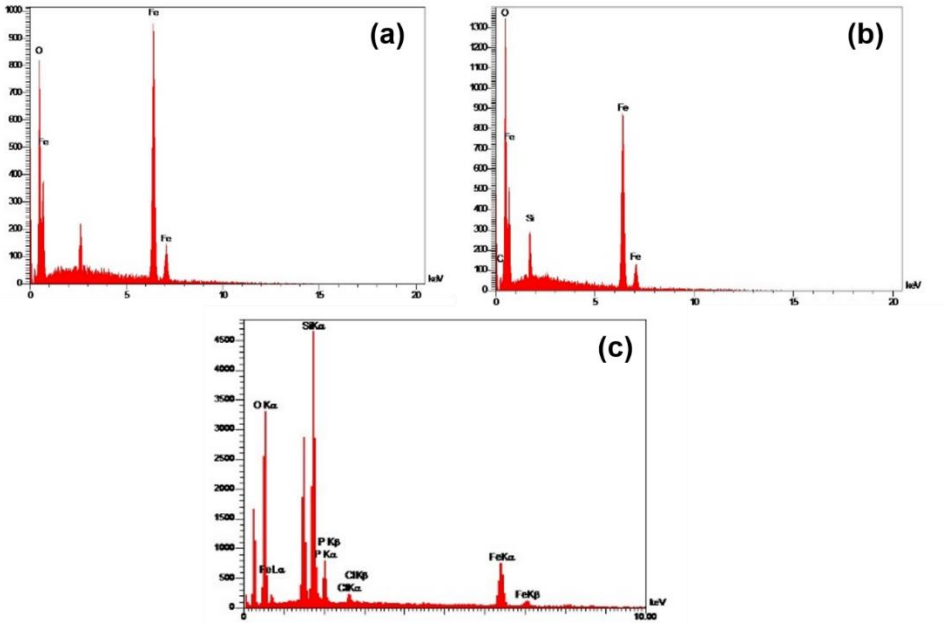

Figure 6. SEM-EDX spectrum: (**a**) Fe_3O_4, (**b**) Fe_3O_4@SiO_2, (**c**) Fe_3O_4@SiO_2–O–PCl_2

Table 1. EDX elemental composition of Fe_3O_4@SiO_2–O–PCl_2

Elt	Line	Int	Error	K	Kr	W%	A%	ZAF
O	Ka	47.8	309.2931	0.1238	0.1102	14.33	32.41	0.7694
Si	Ka	153.9	57.6089	0.1536	0.1368	15.30	19.72	0.8937
P	Ka	27.8	58.4499	0.0330	0.0294	3.35	3.92	0.8764
Cl	Ka	9.4	6.2485	0.0153	0.0136	1.45	1.48	0.9379
Fe	Ka	48.6	0.8631	0.6744	0.6007	65.56	42.48	0.9162
Total		**100.00**		1.0000	0.8907	100.00	100.00	

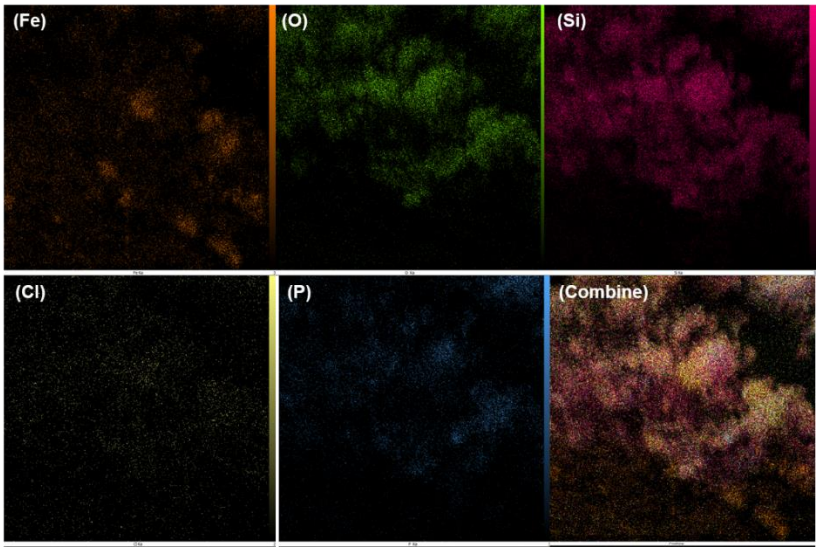

Figure 7. EDX-Mapping analysis of Fe_3O_4@SiO_2–O–PCl_2

3.1.5. Magnetic properties

VSM analysis (**Figure 8**) gave saturation magnetization (M_s) values of 58.36, 22.85, and 19.86 emu g^{-1} for Fe_3O_4, Fe_3O_4@SiO_2, and the final catalyst, respectively. The decrease is attributed to the non-magnetic silica and phosphorus layers, which dilute the magnetic core. The absence of hysteresis in all samples confirms superparamagnetic behavior [39], enabling easy magnetic separation with an external magnet.

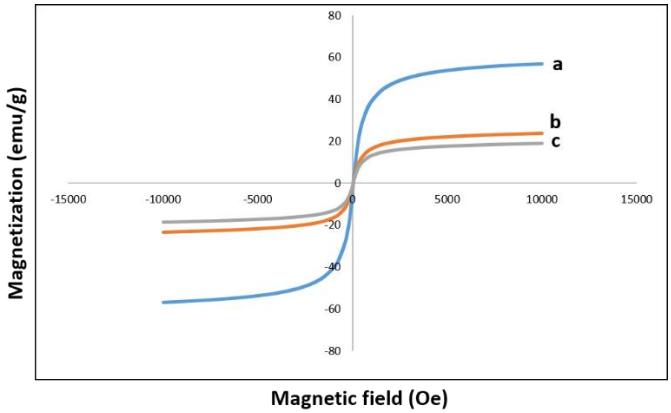

Figure 8. Magnetization curves for (**a**) Fe_3O_4, (**b**) Fe_3O_4@SiO_2, (**c**) Fe_3O_4@SiO_2–O–PCl_2

3.2. Optimization of reaction conditions

A model reaction using 4-methylbenzaldehyde, isatin, and ammonium acetate in ethanol was employed for optimization (**Table 2**). Various catalysts were screened; the magnetic nanocatalyst Fe_3O_4@SiO_2–O–PCl_2 gave the best results (Entry 9, 90% yield in 1 h). The optimal catalyst amount was 40 mg; higher amounts did not improve yield. Ethanol was the best solvent, and reflux temperature (~78 °C) was optimal. Entry 20 in **Table 2** has been corrected to "reflux" (not 110 °C), as ethanol's boiling point is approximately 78 °C. The reaction did not proceed at room temperature (trace product) and gave lower yields at 60 °C (78%).

Table 2. Optimization of reaction conditions

Entry	Catalyst (mg)	Temperature (°C)	Solvent	Time (h)	Yield (%)[b]
1	-	reflux	EtOH	12	51
2	$AlCl_3$ (40)	reflux	EtOH	4	45
3	$BiCl_3$ (40)	reflux	EtOH	4	64
4	$FeCl_3$ (40)	reflux	EtOH	4	47
5	$ZnCl_2$ (40)	reflux	EtOH	4	58
6	$MnCl_2$ (40)	reflux	EtOH	4	55
7	SPION (40)	reflux	EtOH	4	67
8	PCl_3 (40)	reflux	EtOH	4	44
9	Fe_3O_4@SiO_2–O–PCl_2 (40)	reflux	EtOH	1	90
10	Fe_3O_4@SiO_2–O–PCl_2 (20)	reflux	EtOH	4	55
11	Fe_3O_4@SiO_2–O–PCl_2 (30)	reflux	EtOH	1	75
12	Fe_3O_4@SiO_2–O–PCl_2 (50)	reflux	EtOH	1	90
13	Fe_3O_4@SiO_2–O–PCl_2 (40)	reflux	H_2O	1	65
14	Fe_3O_4@SiO_2–O–PCl_2 (40)	reflux	EtOH/ H_2O	1	80
15	Fe_3O_4@SiO_2–O–PCl_2 (40)	reflux	$CHCl_3$	1	45
16	Fe_3O_4@SiO_2–O–PCl_2 (40)	reflux	DMF	1	40
17	Fe_3O_4@SiO_2–O–PCl_2 (40)	reflux	Toluene	1	71
18	Fe_3O_4@SiO_2–O–PCl_2 (40)	r.t.	EtOH	2	Trace
19	Fe_3O_4@SiO_2–O–PCl_2 (40)	60	EtOH	1	78
20	Fe_3O_4@SiO_2–O–PCl_2 (40)	reflux	EtOH	1	90

[a] Reaction conditions: 4-methylbenzaldehyde (1 mmol), isatin (1 mmol), ammonium acetate (2 mmol). *b* Isolated yield.

3.3. Synthesis of substituted imidazole's (Scope)

Under optimized conditions, a range of aromatic aldehydes with electron-donating (hydroxy, methyl, methoxy) and electron-withdrawing (halogens, cyano, nitro) substituents were converted to the corresponding substituted 2-phenyl-3,4-dihydroimidazo[4,5-b]indoles in good to excellent yields (**Scheme 2**). The reaction proceeded cleanly with no side products, demonstrating the broad substrate tolerance and efficiency of the catalyst.

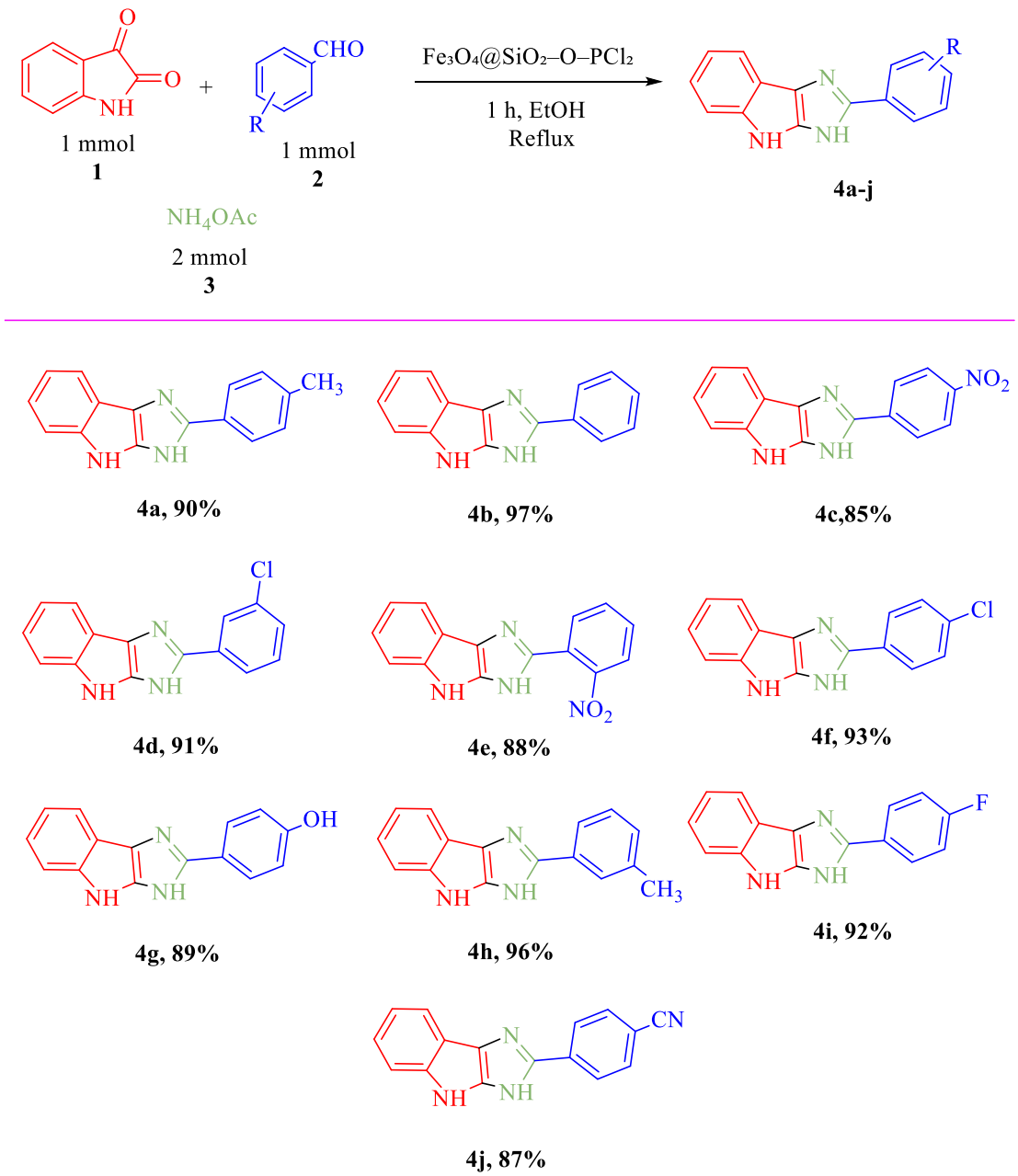

Scheme 2. Synthesis of substituted imidazoles catalyzed by $Fe_3O_4@SiO_2–O–PCl_2$

3.4. Proposed mechanistic pathway

Based on literature precedent [30] and our findings, a mechanism is proposed (**Scheme 3**). The P–O–Si moiety (or residual P–Cl group) acts as a Lewis acid [40], activating the aldehyde carbonyl through coordination, which facilitates nucleophilic attack by ammonium acetate to form imine intermediate A. Dehydration gives iminium ion B, which undergoes nucleophilic addition by isatin to give intermediate C. Finally, proton transfer (from the ammonium nitrogen to the carbonyl oxygen) assisted by the catalyst yields product **4a** and regenerates the catalyst. The Lewis acidic nature of the phosphorus center is responsible for the activation, and the covalent attachment ensures heterogeneity.

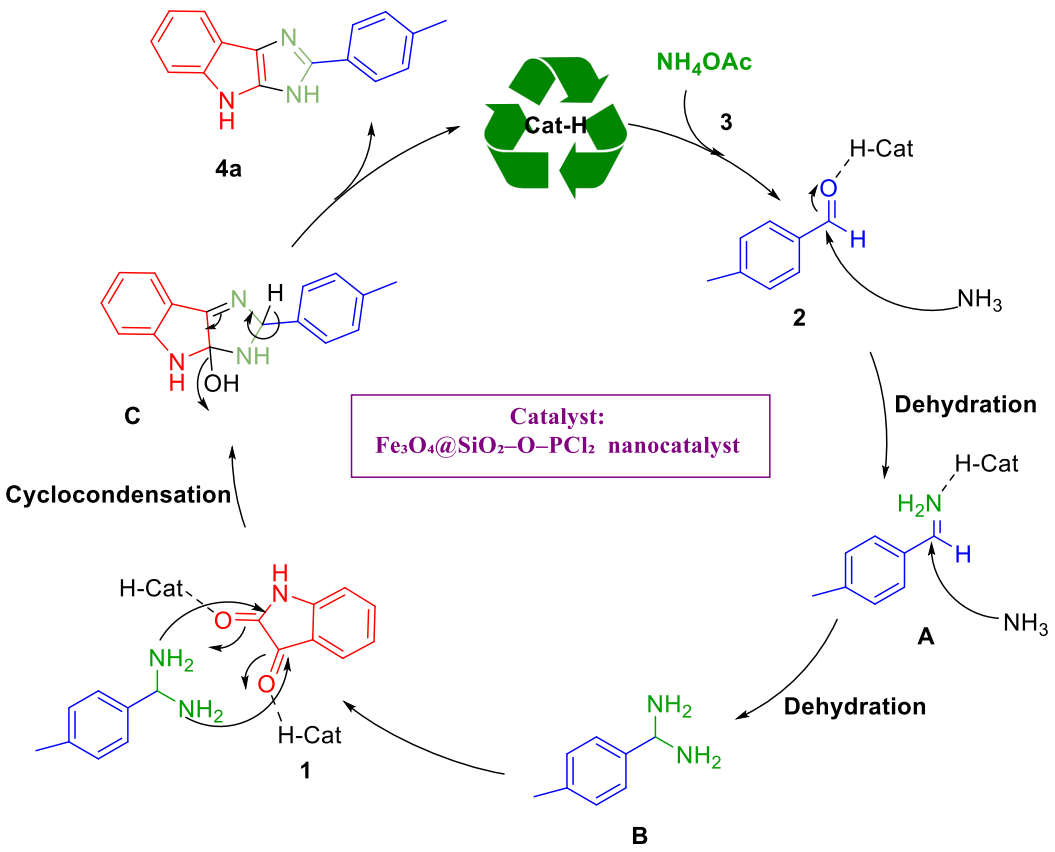

Scheme 3. Proposed mechanism.

3.5. Control experiment with bare support

To confirm the essential role of phosphorus in catalysis, a control reaction was performed using Fe_3O_4@SiO_2 (without PCl_3 functionalization) under identical conditions. Only trace amounts of product (<15% yield) were obtained after 4 h, proving that the phosphorus species are indispensable for high catalytic activity and that the support alone has negligible activity.

3.6. Reusability of the catalyst

The catalyst was recovered by magnetic separation and reused in five consecutive runs (**Table 3**). The yield decreased slightly from 90% to 80%, attributed to minimal leaching of active phosphorus species, surface adsorption of organic residues, and/or particle agglomeration [41]. To investigate this, the recovered catalyst after five runs was analyzed by SEM-EDX (Table 4; full data in Supporting Information), which showed no significant morphological changes or loss of elemental composition (Fe, Si, P, Cl remained consistent within experimental error), confirming good structural stability. The slight decrease in activity is acceptable for practical applications and highlights the robust nature of the catalyst.

Table 3. Reusability data.

Run	1	2	3	4	5
Yield	90	90	88	85	80

Table 4. EDX elemental composition of the recovered Fe_3O_4@SiO_2–O–PCl_2 catalyst after five runs

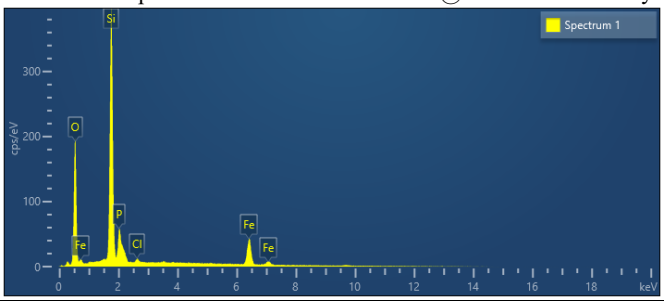

Spectrum 1				
Element	**Line Type**	**Weight %**	**Weight % Sigma**	**Atomic %**
O	K series	56.54	0.24	72.34
Si	K series	28.56	0.18	20.82
P	K series	4.28	0.12	2.83
Cl	K series	0.54	0.05	0.31
Fe	K series	10.07	0.14	3.69
Total		100.00		100.00

4. Conclusion

A novel magnetic nanocatalyst Fe_3O_4@SiO_2–O–PCl_2 was successfully synthesized and fully characterized using FT-IR, XRD, VSM, TGA/DTG, FE-SEM, SEM-EDX, and mapping techniques. It efficiently promotes the one-pot three-component synthesis of substituted 2-phenyl-3,4-dihydroimidazo[4,5-b]indoles from aromatic aldehydes, isatin, and ammonium acetate under mild conditions (ethanol, reflux, 1 h) with high yields (up to 90%). The catalyst shows excellent reusability (5 cycles with only 10% loss of activity) and can be easily recovered using an external magnet, eliminating the need for filtration. The covalent anchoring of phosphorus species to the silica surface ensures stability and prevents leaching, while the use of a catalytic amount of PCl_3 (anchored form) minimizes toxicity concerns. This protocol offers a greener, more practical alternative to existing methods, combining the advantages of homogeneous and heterogeneous catalysis.

Acknowledgment

The authors are thankful to the Islamic Azad University, Marvdasht Branch, for providing laboratory facilities to carry out this research.

Authors' contributions

Somayeh Zare: Research and writing of the original manuscript. Arezu Jamalian: Corresponding author and manuscript editing. Masoomeh Emadi: Analysis and writing of the original manuscript.

Declaration of competing interest

The authors declare that they have no conflict of interest.

Funding

This paper received no funding.

Data availability

Data will be made available on request.

References

[1] T. Li, D. Jia, S. Zhou, Z. Liu, J. Chen, T. Ban, H. Gao, Review on recent advances in supported metal catalysts for synthesis of high energy density fuels, Fuel 373 (2024) 132329.
DOI: https://doi.org/10.1016/j.fuel.2024.132329.

[2] J. Liu, R. Burciaga, S. Tang, S. Ding, H. Ran, W. Zhao, W. Zhu, Recent advances in hydrotreating catalyst supports: A review, Innov. Mater. 2(3) (2024) 100090.
DOI: https://doi.org/10.59717/j.xinn-mater.2024.100090.

[3] J.J. Villora-Picó, J. González-Arias, L. Pastor-Pérez, J.A. Odriozola, T.R. Reina, A review on high-pressure heterogeneous catalytic processes for gas-phase CO_2 valorization, Environ. Res. 240 (2024) 117520.
DOI: https://doi.org/10.1016/j.envres.2023.117520.

[4] S. Rostamnia, E. Doustkhaha, Increased SBA-15-SO3H catalytic activity through hydrophilic/hydrophobic fluoroalkyl-chained alcohols (RFOH/SBA-15–Pr-SO3H), Synlett 26 (2015) 1345. **DOI**: https://doi.org/10.1055/s-0034-1380683.

[5] T. Cheng, D. Zhang, H. Li, G. Liu, Magnetically recoverable nanoparticles as efficient catalysts for organic transformations in aqueous medium, Green Chem. 16 (2014) 3401. **DOI**: https://doi.org/10.1039/c4gc00458b.

[6] D. Astruc, F. Lu, J.R. Aranzaes, Nanoparticles as recyclable catalysts: The frontier between homogeneous and heterogeneous catalysis, Angew. Chem. Int. Ed. 44 (2005) 7852.
DOI: https://doi.org/10.1002/anie.200500766.

[7] N. Alishahi, M. Nasr-Esfahani, I. Mohammadpoor-Baltork, S. Tangestaninejad, V. Mirkhani, M. Moghadam, Nicotine-based ionic liquid supported on magnetic nanoparticles: An efficient and recyclable catalyst for selective one-pot synthesis of mono- and bis-4H-pyrimido[2,1-b]benzothiazoles, Appl. Organomet. Chem. 34(8) (2020) e5681.
DOI: https://doi.org/10.1002/aoc.5681.

[8] G. Peng, J. Zhou, J. Tao, W. Wang, J. Liu, J. Yao, Z. Yao, Magnetic nanoparticle-modified hollow double-shell SiC@C@FeCo with excellent electromagnetic wave absorption, Nano Res. 17(4) (2024) 3164.
DOI: https://doi.org/10.1007/s12274-023-6084-1.

[9] H.A. Younus, M. Al-Rashida, A. Hameed, M. Uroos, U. Salar, S. Rana, K.M. Khan, Multicomponent reactions (MCR) in medicinal chemistry: A patent review (2010–2020), Expert Opin. Ther. Pat. 31(3) (2021) 267.
DOI: https://doi.org/10.1080/13543776.2021.1858797

[10] F. Brunelli, F. Quartieri, I. Miletto, M. Pulici, G. Papeo, G.C. Tron, Visible light promoted site-specific functionalization of α-acyloxy carboxamides: Unlocking a forbidden chemical space in the Passerini reaction, Chem. Eur. J. 30(50) (2024) e202402175.
DOI: https://doi.org/10.1002/chem.202402175.

[11] S. Zheng, H. Huang, C. Guan, L. Zhang, L. Xiao, J. Pang, J. Chen, L. Wang, Role of catechin on furfural inhibition in sugarcane juice during thermal treatment: Adducts and mechanism, Food Control 160 (2024) 110364.
DOI: https://doi.org/10.1016/j.foodcont.2024.110364.

[12] M. Faizan, R. Kumar, A. Mazumder, Salahuddin, N. Kukreti, P.K. Tyagi, B. Kapoor, Hantzsch reaction: The important key for pyridine/dihydropyridine synthesis, Synth. Commun. 54(15) (2024) 1221.
DOI: https://doi.org/10.1080/00397911.2024.2337090.

[13] A. Chandravarkar, T. Aneeja, G. Anilkumar, Advances in Biginelli reaction: A comprehensive review, J. Heterocycl. Chem. 61(1) (2024) 5.
DOI: https://doi.org/10.1002/jhet.4746.

[14] B. Ganem, Strategies for innovation in multicomponent reaction design, Acc. Chem. Res. 42(3) (2009) 463.
DOI: https://doi.org/10.1021/ar800214s.

[15] B.H. Rotstein, S. Zaretsky, V. Rai, A.K. Yudin, Small heterocycles in multicomponent reactions, Chem. Rev. 114(16) (2014) 8323.
DOI: https://doi.org/10.1021/cr400615p.

[16] F.-F. Zhang, L.-L. Gan, C.-H. Zhou, Synthesis, characterization and biological evaluation of novel imidazole derivatives, Bioorg. Med. Chem. Lett. 20 (2010) 1881.
DOI: https://doi.org/10.1016/j.bmcl.2010.01.135.

[17] F. Sa˛czewski, T. De˛bowski, M. Gdaniec, J. Petrusewicz, M. Turowski, B. Damasiewicz, Synthesis, structure and antiaggregatory effects of some α-hydroxy analogues of 2-aryliminoimidazolines in human platelets, Eur. J. Pharm. Sci. 4 (1996) 85.
DOI: https://doi.org/10.1016/0928-0987(95)00041-0.

[18] F. Sa˛czewski, T. De˛bowski, J. Petrusewicz, H. Trzeciak, E. Krzystanek, M. Krzystanek, M. Gdaniec, E. Nowakowska, Synthesis, structure and biological activities of some N-(4,5-dihydro-1H-imidazol-2-yl)-1,3-dihydrobenzimidazole derivatives, Arch. Pharm. Pharm. Med. Chem. 331 (1998) 241.
DOI: https://doi.org/10.1002/(SICI)1521-4184(199807)331:7/8<241::AID-ARDP241>3.0.CO;2-K.

[19] J. Grant, M.C. Scrutton, Novel α_2-adrenoreceptors primarily responsible for inducing human platelet aggregation, Nature 227 (1979) 659.
DOI: https://doi.org/10.1038/227659a0.

[20] C.H. Ahn, A. Hamada, D.D. Feller, Alpha-adrenoreceptor-mediated actions of optical isomers and deoxy analogs of catecholimidazoline and norepinephrine in human platelets, Biochem. Pharmacol. 35 (1986) 4095.
DOI: https://doi.org/10.1016/0006-2952(86)90019-3.

[21] R.M. Eglen, A.L. Hudson, D.A. Kendall, D.J. Nutt, N.G. Morgan, V.G. Wilson, M.P. Dillon, Seeing through a glass darkly: Casting light on imidazoline I sites, TiPS 19 (1998) 381.
DOI: https://doi.org/10.1016/S0165-6147(98)01237-2.
[22] C.Y. Hsu, D.R. Knapp, P.V. Halushka, The effects of α-adrenergic agents on human platelet aggregation, J. Pharmacol. Exp. Ther. 208 (1979) 366.
DOI: https://doi.org/10.1016/S0022-3565(25)31581-8.
[23] Y.A. Ding, D.E. McIntyre, C.I. Keynon, P.F. Semple, Potentiation of adrenaline-induced platelet aggregation by angiotensin II, Thromb. Haemost. 54 (1985) 717.
DOI: https://doi.org/10.1055/s-0038-1660105
[24] G.V.M. Sharma, Y. Jyothi, P.S. Lakshmi, Efficient room-temperature synthesis of tri- and tetrasubstituted imidazoles catalyzed by $ZrCl_4$, Synth. Commun. 36 (2006) 2991.
DOI: https://doi.org/10.1080/00397910600773825.
[25] L.M. Wang, Y.H. Wang, H. Tian, Y.F. Yao, J.H. Shao, B. Liu, Ytterbium triflate as an efficient catalyst for one-pot synthesis of substituted imidazoles through three-component condensation of benzil, aldehydes and ammonium acetate, J. Fluorine Chem. 127 (2006) 1570.
DOI: https://doi.org/10.1016/j.jfluchem.2006.09.005.
[26] S. Bajpai, S. Singh, V. Srivastava, Nano zirconia catalysed one-pot synthesis of some novel substituted imidazoles under solvent-free conditions, RSC Adv. 5 (2015) 28163.
DOI: https://doi.org/10.1039/C4RA16211K.
[27] S.N. Shelke, G.R. Mhaske, V.D. Bonifacio, M.B. Gawande, Green synthesis and anti-infective activities of fluorinated pyrazoline derivatives, Bioorg. Med. Chem. Lett. 22 (2012) 5727.
DOI: https://doi.org/10.1016/j.bmcl.2012.06.072.
[28] S. Damavandi, R. Sandaroos, L-Proline-catalyzed three-component synthesis of condensed imidazoles, Arab. J. Chem. 9 (2016) S1138.
DOI: https://doi.org/10.1016/j.arabjc.2011.12.018.
[29] R.S. Joshi, P.G. Mandhane, M.U. Shaikh, R.P. Kale, C.H. Gill, Potassium dihydrogen phosphate catalyzed one-pot synthesis of 2,4,5-triaryl-1H-imidazoles, Chin. Chem. Lett. 21 (2010) 429.
DOI: https://doi.org/10.1016/j.cclet.2009.11.012.
[30] A.S. Nipate, C.K. Jadhav, A.V. Chate, K.S. Taur, C.H. Gill, β-Cyclodextrin catalyzed access to fused 1,8-dihydroimidazo[2,3-b]indoles via one-pot multicomponent cascade in aqueous ethanol: Supramolecular approach toward sustainability, J. Heterocycl. Chem. 57(2) (2020) 820.
DOI: https://doi.org/10.1002/jhet.3819.
[31] M.U. Khan, Z.N. Siddiqui, Ce@STANPs/ZrO_2 as nanocatalyst for multicomponent synthesis of isatin-derived imidazoles under green reaction conditions, ACS Omega 3(8) (2018) 10357.
DOI: https://doi.org/10.1021/acsomega.8b01043.
[32] N. Iranpoor, H. Firouzabadi, A. Jamalian, M. Tamami, Silphos [PCl_3−n(SiO_2)n], a heterogeneous phosphine reagent mediated the conversion of oximes to nitriles and amides or carbonyl compounds, Lett. Org. Chem. 3(4) (2006) 267.
DOI: https://doi.org/10.2174/157017806776980014.
[33] R.A. Nyquist, R.O. Kagel, Infrared Spectra of Inorganic Compounds, Academic Press, New York, 1971. ISBN: 9780125234508.
[34] A.L. Smith, Analysis of Silicones, Wiley-Interscience, New York, 1974. ISBN: 0471800104.
[35] L.J. Bellamy, The Infra-red Spectra of Complex Molecules, Chapman and Hall, London, 1980. ISBN: 0412223503.
[36] G. Socrates, Infrared and Raman Characteristic Group Frequencies, 3rd ed., John Wiley & Sons, Chichester, 2001. ISBN: 9780471852988.
[37] P. Gabbott, Principles and Applications of Thermal Analysis, Blackwell Publishing, Oxford, 2008. ISBN: 9781405131711.
[38] JCPDS Card No. 85-1436 (Fe_3O_4), International Centre for Diffraction Data, 2000.
[39] S. Sunkara, D. Sravanthi, K.M. Maheswari, S. Salma, B.N. Nallur, Development of modified release tablet dosage forms of capecitabine for better therapeutic efficacy, J. Chem. Pharm. Res. 5 (2013) 320.
[40] M.B. Smith, March's Advanced Organic Chemistry, 8th ed., Wiley, Hoboken, 2020. ISBN: 9781119371809.
[41] J.M. Thomas, W.J. Thomas, Principles and Practice of Heterogeneous Catalysis, VCH, Weinheim, 1997. ISBN: 3527292888.